



Modeling scintillation light absorption and re-emission in SrI₂(Eu) scintillators

H. Tan*, W.K. Warburton

XIA LLC, 31057 Genstar Rd., Hayward, CA 94544, USA

ARTICLE INFO

Available online 19 January 2011

Keywords:

Strontium iodide
Light trapping
Energy resolution
Decay time variations

ABSTRACT

Europium-doped strontium iodide has recently attracted interest as a scintillator for gamma-ray spectroscopy. Excellent energy resolution (2.6% FWHM at 662 keV) with SrI₂(Eu) has been reported for small (< 1 cm³) crystals. With larger crystals, however, substantial energy resolution degradation has been found. Proposed as a mechanism for explaining this phenomenon, “light trapping” suggests that scintillation photons generated in SrI₂(Eu) could be absorbed back into the excited states of the Eu²⁺ activators and then re-emitted at a later time, thus prolonging the pulse decay time as well as increasing the probabilities of losses within the crystal bulk and at the interface of the crystal with outer reflectors. Varying pulse decay times and absorption losses would then produce varied pulse heights from pulse processing electronics with a fixed shaping time. In this paper we report an approach to modeling this “light trapping” mechanism, hoping to produce an explicit description of the connection between the trapping rate and increases and/or variations in decay times. Our model shows that decay times depend strongly on the ratio *R* of SrI₂(Eu)’s optical absorption length to crystal dimension, with smaller *R* values producing longer decay times. Further, decay curves for small *R* values were best characterized by two decay components, whereas those from larger *R* values had only one. Using these results, we devised a digital pulse processing algorithm that can correct for decay time variations with better than 2% accuracy, offering an approach to recovering SrI₂(Eu)’s inherently excellent energy resolution.

© 2011 Elsevier B.V. All rights reserved.

1. Introduction

With the goal of unambiguous radioisotope identification using gamma-ray spectroscopy, researchers in the last few decades had been searching for new scintillator materials that not only can offer energy resolution of ~2% at 662 keV but also are growable to large volumes at low cost. Currently, LaBr₃(Ce) is the commercially available inorganic scintillator that offers the best energy resolution (~2.6% at 662 keV) but it has undesired intrinsic radioactivity and it is still challenging to grow it into large crystals. Europium-doped strontium iodide SrI₂(Eu) has recently attracted interest as a scintillator for gamma-ray spectroscopy [1]. It has a light yield in excess of 100,000 photons/MeV, light yield proportionality better than LaBr₃(Ce), an excellent energy resolution of 2.6% at 662 keV, at least for small (< 1 cm³) crystals, and is easy to grow into large crystals. With larger crystals, however, substantial energy resolution degradation was found [2], in association with decay times that varied on

a pulse-by-pulse basis. Since the Eu optical absorption and emission bands strongly overlap in SrI₂(Eu), “light trapping” has been proposed as a mechanism for explaining this behavior [2]. In this model, scintillation photons generated in SrI₂(Eu) could be absorbed back into the excited states of the Eu²⁺ activators and then re-emitted at a later time, thus prolonging the pulse decay time as well as increasing the probabilities of losses within the crystal bulk and at the interface of the crystal with outer reflectors. Varying pulse decay times and absorption losses would then produce varied pulse heights in pulse processing electronics with a fixed shaping time, therefore degrading energy resolution. While energy resolution degradation and its position dependence in large SrI₂(Eu) crystals had been experimentally confirmed [2], no systematic analysis has been done to explore the possible relationship between the proposed light trapping mechanism and decay time variations in SrI₂(Eu) crystals.

This study offers an approach to modeling this mechanism that we developed with the goals of producing both an explicit description of the connection between the light trapping rate and increases and/or variations in decay times and, hopefully, of also designing a digital pulse processing algorithm that would allow us to recapture the material’s excellent energy resolution. In our model, we first divided a cylindrical SrI₂ crystal into a given

* Corresponding author.

E-mail address: htan@xia.com (H. Tan).

number of voxels, and then used the ray-tracing Monte Carlo program DETECT2000 [3] to compute an absorption matrix that gives the probability that a scintillation photon emitted from one voxel is absorbed in another voxel as it propagates through the scintillator. Next we calculated a scintillation decay curve for each voxel by propagating photons from that voxel throughout the crystal and into the PMT as a function of time. From the decay curves, we derived the decay time, or times, associated with each voxel and thus the distribution of decay times from the crystal as a whole. This distribution not only illustrates the effect of light trapping rate of different voxels on their decay times but also enables us to devise a digital pulse processing algorithm that can correct decay time variations with better than 2% accuracy. Finally, we compared our simulation results to those reported in the literature.

2. Materials and methods

2.1. Modeling with DETECT2000

Fig. 1 shows a sketch of the modeling geometry for DETECT2000. A 1" × 1" SrI₂(Eu) cylindrical crystal was divided into 200 voxels, with 10 divisions in X-axis direction and 20 divisions in the Z-axis direction. Each voxel is an annulus about the Z-axis with a constant cross-section in the X-Z plane. In DETECT2000, scintillation photons were generated isotropically at the center of each voxel and then tracked as the photons propagated through the volume of the crystal until they either (1) reached the PMT surface (detected) or (2) were absorbed in the bulk of the crystal (bulk absorbed), or (3) were absorbed at the outer reflectors (surface absorbed). From the DETECT2000 results, we computed an absorption matrix, $R_{i,j}$, which gives the probability that a photon emitted from voxel i is absorbed in voxel j without escaping the crystal, i.e., without being detected or surface absorbed. For this, we had to modify the DETECT2000 source code slightly since the original code terminates a photon at the starting location of a trajectory when it determines that the photon will be bulk absorbed along the trajectory. We instead used the following formula to compute the distance that the photon would travel along the trajectory before being absorbed:

$$d = -\lambda * \ln(1 - r * (1 - e^{-L/\lambda})) \tag{1}$$

where λ is the bulk absorption length of SrI₂(Eu), L is the trajectory length, r is a random number between 0 and 1, and d is the distance the photon will be able to travel along the trajectory before it is bulk absorbed. Using the current location of the photon and the computed trajectory distance d , we thus were able to specify the voxel wherein the bulk absorption occurred.

When generating the definition file for DETECT2000, we chose the following optical properties for the SrI₂(Eu) crystal: index of refraction was 1.85; the side and top surfaces of the crystal had PAINT finish with a reflection coefficient of 0.98; the bulk absorption mean free path was varied from 25.4 to 1625.6 mm in seven discrete steps to study the light trapping mechanism; the scattering mean free path was set to -1 , i.e., no photon scattering is simulated. The bottom surface of the crystal was coupled to PMT through a thin (0.2 mm) layer of optical couplant. The index of refraction of both the PMT window (1 mm thick) and the optical couplant layer were set to 1.50. The optical finish of the surfaces between the PMT window, optical layer, and the bottom surface of the crystal was POLISH, whereas that of the cylindrical surfaces of the PMT window and optical couplant was METAL

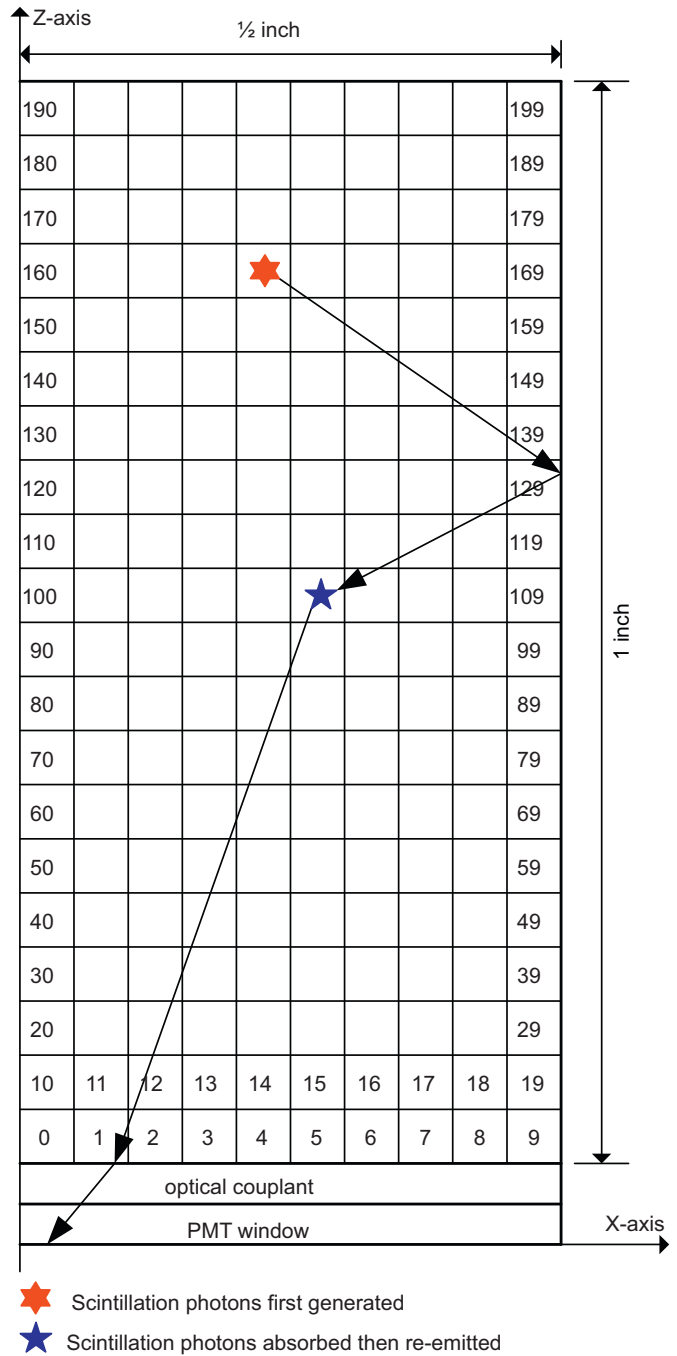


Fig. 1. Sketch showing a 1" × 1" SrI₂(Eu) cylindrical crystal divided into 200 voxels. Each voxel is an annulus about the Z-axis with a constant cross section in the X-Z plane.

with a reflection coefficient of 1.0. The bottom surface of the PMT window was DETECT with unity quantum efficiency.

2.2. Derivation of decay times

Using the absorption matrix, next we calculated a scintillation decay curve for each voxel by propagating photons from an event originating within the volume of that voxel throughout the crystal and into the PMT as a function of time, including an optional re-emission efficiency at each time step. A non-unity re-emission efficiency means loss of photons during the absorption and then

re-emission process. Letting $N_i(t)$ be the number of excited states in voxel i at time t , we can write the time evolution of $N_i(t)$ as:

$$\frac{dN_i(t)}{dt} = -\alpha * N_i(t) + \alpha * \epsilon * \sum_j (N_j(t) * R_{ij}) \quad (2)$$

where α is the inverse of the nominal decay time constant of $\text{SrI}_2(\text{Eu})$, ϵ is the re-emission efficiency, and R_{ij} is the computed absorption matrix. The nominal $\text{SrI}_2(\text{Eu})$ decay time was set to $1 \mu\text{s}$ for all computations.

From the computed decay curves, we derived the decay time, or times if the decay curve has more than one decay components, associated with each voxel and thus the distribution of decay times from the crystal as a whole. Defining a scaling factor R as the ratio of bulk absorption length (or bulk mean free path as defined in DETECT2000) λ to crystal dimension D (crystal diameter or height), we then repeated the calculations for a total of 7 different values of R ranging from 1 to 64. We also varied the re-emission efficiency ϵ to investigate how it would affect the decay times.

3. Results and discussions

3.1. Effect of scaling factor

Fig. 2 shows, for the 7 values of scaling factor R ($R=1, 2, 4, 8, 16, 32, \text{ and } 64$), decay curves from five voxels (#2, 52, 102, 152, and 192) were selected to display the range of computed behaviors. Only the first 8 μs of the decay curves were shown since after about 6 μs all the voxels for a particular R value decay similarly, with the same decay constant. We first observe that the resulting decay times depend strongly on R , with smaller R values producing longer decay times. Further, decay curves for small R values ($R=1$ to 8) are best characterized by two decay components, whereas those from larger R values ($R=16$ to 64) have only one. We further observe that as R becomes smaller, the range of decay time values seen across the crystal increases.

3.2. Effect of re-emission efficiency

Fig. 3 illustrates the effects of re-emission efficiency ϵ on decay times. Decay curves from voxel #102 were chosen for this

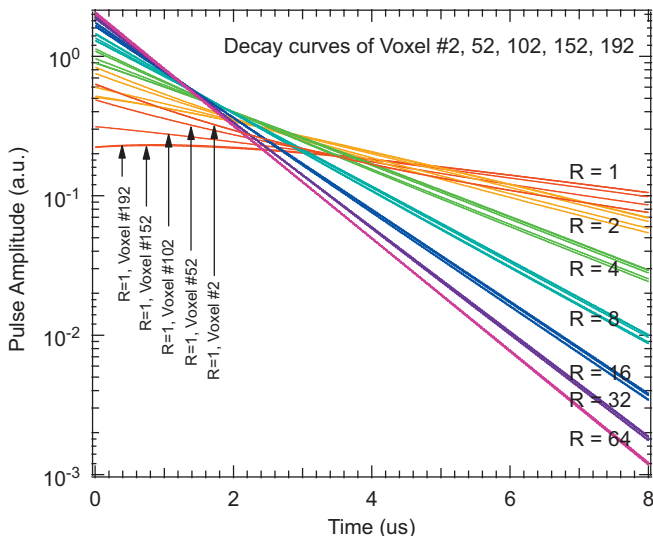


Fig. 2. Decay curves of five selected voxels at different scaling factor R .

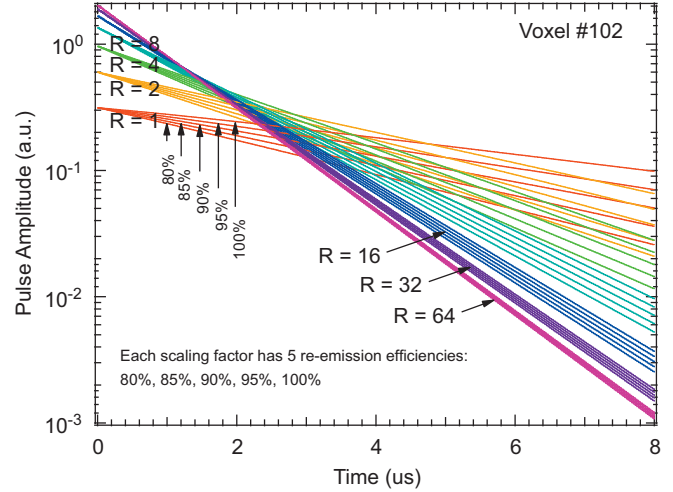


Fig. 3. Decay curves from voxel #102 at different re-emission efficiencies ϵ and different scaling factor R .

analysis. Each of the seven R ratios has five ϵ values: 80, 85, 90, 95, and 100%, respectively. Within each R ratio, a smaller ϵ gives a smaller decay time, and this behavior becomes more pronounced for low R values. For instance, at ratio $R=1$, the decay time (the longer one of the two decay components) varies from 3.1 μs at 80% to 6.4 μs at 100%, whereas at ratio $R=64$, the single decay time varies from 1.06 μs at 80% to 1.08 μs at 100%.

3.3. Decay time distributions

Fig. 4 shows the distribution of decay times for all 200 voxels with $R=2$ and $\epsilon=100\%$. The two decay components of each voxel are represented by square and circle marks, respectively. Component #1 varied between 1.5 and 5 μs whereas component #2 had a tight range of 3.50 to 3.60 μs . Decay time component #1 generally increases from the bottom to the top of the crystal, since photons generated in voxels at the top part of the crystal would take longer to propagate through the crystal due to their absorption and then re-emission. There are a few voxels (#49, 59, 68, 69, 77, 86), whose decay time component #1 is as high as 5 μs , which appears to arise from the fact that the decay behavior of these voxels is not well described by a curve fit using two exponential decay components.

At large R values, voxels can be best characterized by one decay component, with only a small variation of decay time between voxels. This is illustrated in Fig. 5 that shows the distribution of decay times for all 200 voxels with $R=64$ and $\epsilon=100\%$. The decay times varied between 1.067 and 1.081 μs , and they were very close to the nominal 1 μs decay time. This model thus attributes the decay time and energy resolution variations observed between small and large $\text{SrI}_2(\text{Eu})$ samples to reductions in R value as crystal size increases.

3.4. Digital pulse correction algorithm

We devised a digital pulse correction algorithm that can correct for decay time variations with better than 2% accuracy, offering an approach to recovering $\text{SrI}_2(\text{Eu})$'s inherently excellent energy resolution. First, we computed two integrals for each voxel's specific decay curve: the first (Int_{0-3}) being the integral over 0–3 μs of the decay curve; the second (Int_{3-6}) being the integral over 3–6 μs of the decay curve. We then designated the

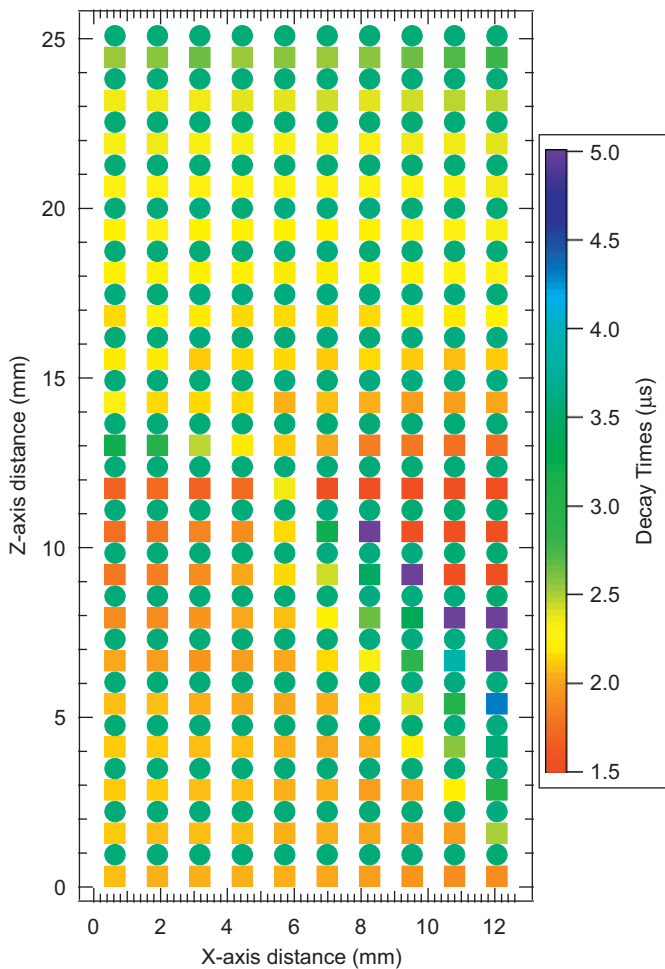


Fig. 4. Distribution of decay times at all 200 voxels with $R=2$ and $\epsilon=100\%$. Each voxel has two decay times represented by square and circle marks, respectively.

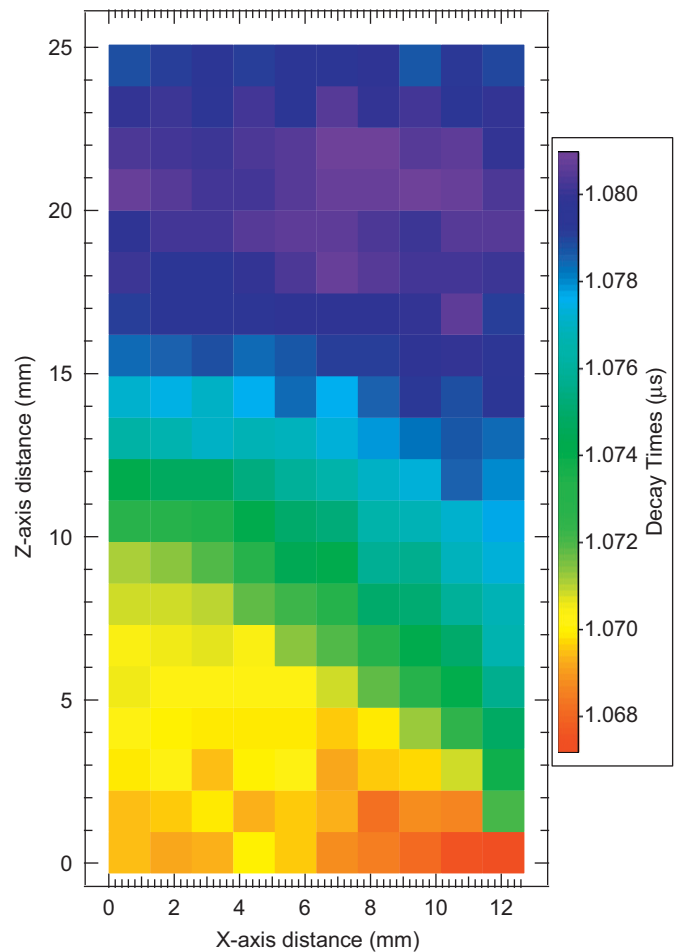


Fig. 5. Distribution of decay times at all 200 voxels with $R=64$ and $\epsilon=100\%$. Each voxel has just one decay time.

ratio of Int_{0-3} to Int_{3-6} as a particle identifier (PID) of the decay curve, and the sum, (Int_{0-6}) , of Int_{0-3} and Int_{3-6} as a representation of pulse energy. After plotting Int_{0-6} versus PID for the decay curves from all voxels at a given scaling ratio R , we fitted the resulting distribution with 4th order polynomial of Int_{0-6} versus PID. We then generated a correction term $\delta\text{Int}_{0-6} = \langle \text{Int}_{0-6} \rangle - \overline{\text{Int}_{0-6}}$ as a function of PID, where $\langle \text{Int}_{0-6} \rangle$ is the value of Int_{0-6} of each voxel and $\overline{\text{Int}_{0-6}}$ is the volume weighted average value of Int_{0-6} over all voxels. Fig. 6 shows Int_{0-6} before and after correction for all scaling ratios R . Its inset illustrates the 4th polynomial fit and average energy for $R=8$. Finally, in Fig. 7 we histogrammed the residual errors between corrected Int_{0-6} values and $\overline{\text{Int}_{0-6}}$ for all voxels at each scaling ratio R . As Fig. 7 clearly shows, all correction errors are below $\pm 2\%$, with majority of them within $\pm 0.5\%$. We note that, once the polynomial correction formula for a specific crystal has been determined, such digital corrections can be easily carried out in real time thereafter using a floating point digital signal processor.

3.5. Comparison to experimental results reported in literature

Cherepy et al. reported position-dependent energy resolution measurements in a 24 cm^3 $\text{SrI}_2(\text{Eu})$ crystal using a collimated ^{137}Cs source [2]. As shown in their Figure 4, events in the top part of the crystal produce much lower pulse heights than do events in the middle or bottom part of the crystal. Further, their

Figure 5 shows that the 662 keV pulse height peak position is nearly inversely proportional to the measured decay time. These are exactly consistent with our simulation results, e.g., Fig. 2. The measured energy resolution differs by more than a factor of 2 in their 24 cm^3 $\text{SrI}_2(\text{Eu})$ crystal when it is measured at the bottom and top of the crystal. From our results we would therefore infer a scaling ratio R of 2 or less, since Fig. 2 shows large decay time variations only for values of $R=2$ or 1. This, in turn, would set an upper limit on the bulk absorption length in $\text{SrI}_2(\text{Eu})$ to be about 6 cm.

The above comparisons are conceptual only, since we so far do not have access to real $\text{SrI}_2(\text{Eu})$ pulses. We are presently working to obtain pulse data from the authors of Ref. [2], with the goal analyzing the pulses and comparing our simulation results to measured pulse results. In particular, we will test our digital pulse correction algorithm on real $\text{SrI}_2(\text{Eu})$ pulses to evaluate its performance.

4. Summary

We have modeled the light trapping mechanism in $\text{SrI}_2(\text{Eu})$ in an effort to develop an understanding of the source of decay time variations in such scintillators. We found that the shape of $\text{SrI}_2(\text{Eu})$ decay curves depends strongly on the relative ratio of its bulk absorption length to the crystal dimensions, with smaller ratio producing longer decay times. Also, at smaller ratios, decay time varies more widely throughout the volume of the crystal,

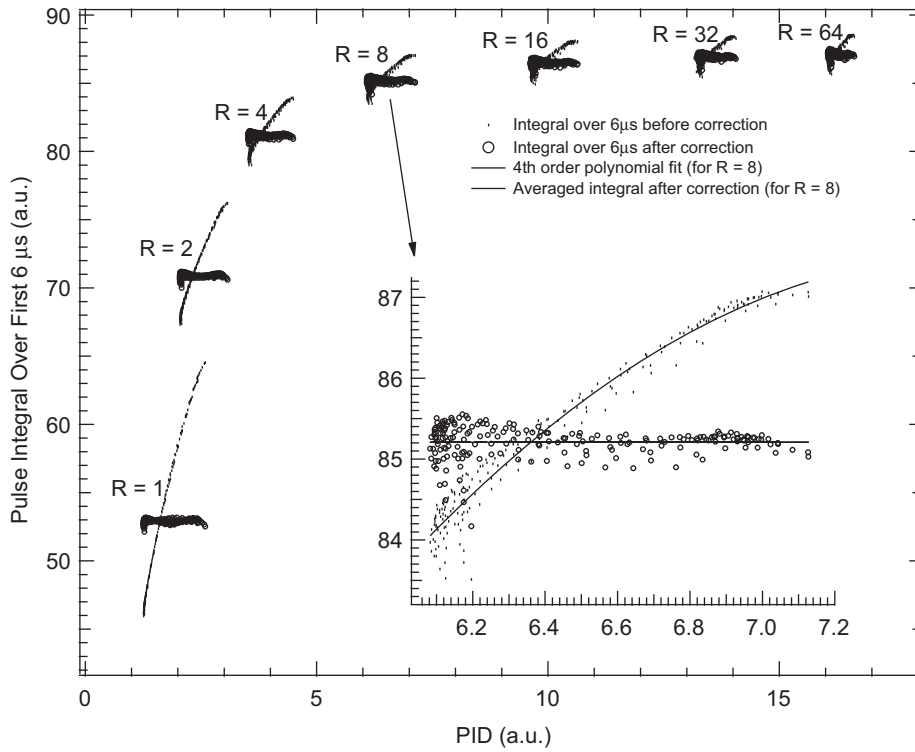


Fig. 6. Pulse integral over the first 6 μs before and after the digital correction as a function of PID for all scaling factors. The inset shows the details of scaling ratio 8: the 4th polynomial fit to the integral before the correction and the average integral after the correction.

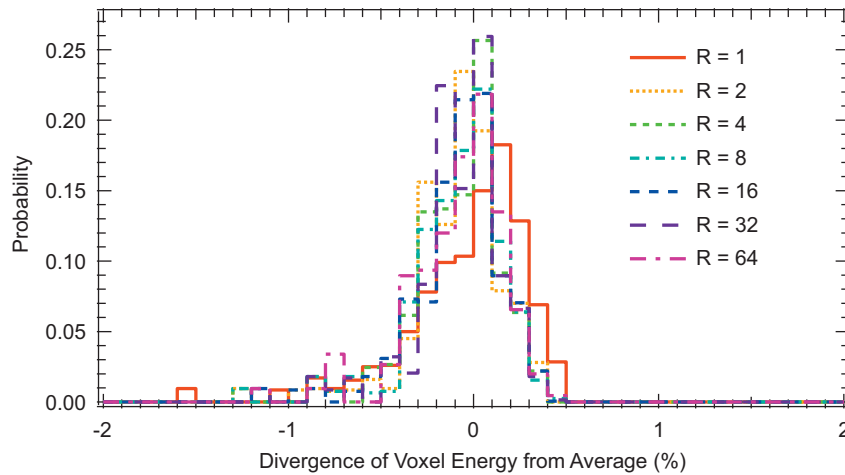


Fig. 7. Digital correction error as represented by the divergence of voxel energy from average for all scaling factors.

implying more serious inhomogeneity problem under such conditions. We found that digital pulse processing techniques can be used to correct such defects for better than 2% precision and thus offer an approach to recovering excellent energy resolution in large $\text{SrI}_2(\text{Eu})$ crystals.

References

[1] N.J. Cherepy, et al., Appl. Phys. Lett. 92 (2008) 083508.
 [2] N.J. Cherepy, et al., Proc. SPIE 7449 (2009) 74490F.
 [3] F. Cayouette, D. Laurendeau, C. Moisan, Proc. SPIE 4833 (2003) 69.